JACS
JOURNAL OF THE AMERICAN CHEMICAL SOCIETY

COMMUNICATION

pubs.acs.org/JACS

# Determination of Molecular Configuration by Debye Length Modulation

Aleksandar Vacic,[*,†] Jason M. Criscione,[‡] Nitin K. Rajan,[∥] Eric Stern,[⊥] Tarek M. Fahmy,[‡,§] and Mark A. Reed[*,†,∥]

Departments of [†]Electrical, [‡]Biomedical, [§]Chemical Engineering, and [∥]Applied Physics, Yale University, 15 Prospect Street, New Haven, Connecticut 06511, United States

[⊥]1366 Technologies, 45 Hartwell Avenue, Lexington, Massachusetts 02421, United States

Supporting Information

**ABSTRACT:** Silicon nanowire field effect transistors (FETs) have emerged as ultrasensitive, label-free biodetectors that operate by sensing bound surface charge. However, the ionic strength of the environment (i.e., the Debye length of the solution) dictates the effective magnitude of the surface charge. Here, we show that control of the Debye length determines the spatial extent of sensed bound surface charge on the sensor. We apply this technique to different methods of antibody immobilization, demonstrating different effective distances of induced charge from the sensor surface.

On the basis of similar principles by which ion sensitive field effect transistors operate,[1] silicon nanowire field effect transistor (FET) technology has demonstrated the ability for low-cost, rapid, ultrasensitive and multiplexed detection of multiple biomolecular species,[2−4] cellular functions,[5] and viruses.[6] In label-free detection schemes, the nanowire surface is functionalized with specific receptors capable of recognizing and capturing a specific target molecule.[6] Upon binding, charges on the captured molecules modulate the nanowire's surface potential. This change in the electrical field causes accumulation or depletion of carriers in the FET channel, thus increasing or decreasing nanowire current. In ionic solution, dissolved charged species form an electrical double layer, lowering the effective charge of the biomolecules. This effect is known as Debye screening and has an exponential behavior, $\exp(-x/\lambda_D)$ [7] with a characteristic distance parameter known as the Debye screening length ($\lambda_D$), defined by:

$$\lambda_D = \frac{1}{\sqrt{4\pi l_B \sum_i \rho_i z_i^2}} \quad (1)$$

where $l_B$ is the Bjerrum length (0.7 nm) and $\rho_i$ and $z_i$ are the density and the valence of the $i$-th ionic species. For typical biological buffer solutions (i.e., 1× to 0.1× phosphate buffered saline, PBS), $\lambda_D$ is approximately 0.7−2.2 nm. Experimental studies have demonstrated that these short distances do not significantly affect the detection of small molecules such as DNA or RNA oligonucelotides (∼2 nm).[4,8−10] However, for larger macromolecules, such as antibodies, size suggests that FET-based detection of antigens via specific binding to antibody-functionalized surfaces will be greatly affected by Debye screening.[11] The first experimental demonstration of the effect of Debye screening on nanowire-based biomolecule detection was performed using a biotinylated sensor for specific detection of an avidin ligand.[12] That work demonstrated that buffer conditions ranging from high to low salt concentrations can severely impact detection sensitivity via Debye length screening.

Here, we extend the understanding of the effect of Debye screening from the model biotin−avidin system to antibody−antigen systems. We examine the effects of ionic strength of the sensing buffer on the level of signal obtained upon label-free detection of a model biomarker, the breast cancer biomarker (CA15.3) using silicon "nanoribbon" bioFETs.[13,14]

To demonstrate how antibody orientation on the sensor surface impacts sensing, we use two different immobilization schemes that bind at different termini the antibody to CA15.3. The resulting different antibody arrangements produce different sensor-to-antigen binding site distances, allowing us to perform a detailed study of the effect of charge screening on sensor response.[15] We further develop a correlation between our experimental data with previous theoretical work.[16]

Silicon nanoribbon FETs are fabricated from silicon-on-insulator (SOI) wafers with 25 nm of active silicon and 145 nm of buried oxide layers in a 5-step photolithography (PL) process similar to the ones previously described.[14] Nanoribbon mesas (1 $\mu$m wide and 10 $\mu$m long) are defined during the first PL step using reactive ion etching, followed by a backgate etch (2nd PL step), source and drain implantation (3rd PL step), rapid thermal annealing at (1000 °C) to activate the dopants, Al contacts metallization (4th PL), and passivation (5th PL, Shipley S1813).

To confer amine functionality to the sensor surface, devices were functionalized using 3-aminopropyltrietoxylsilane (APTES) after the 4th PL step. The APTES layer was formed by immersing the wafers in 5% (v/v) APTES in toluene for 2 h in a nitrogen atmosphere. To improve the monolayer stability, wafers were baked at 180 °C for 2 h in a vacuum oven.[17]

Devices were diced into 5 mm × 5 mm dies, packaged into a 28 pin chip holder (Spectrum Semiconductor Materials, Inc., CSB02892), and wirebonded (West Bond 747677-E79). A custom-made mixing chamber (∼30−40 $\mu$L) using Tygon tube was mounted on the chip using epoxy. Devices were

**Received:** December 27, 2010
**Published:** August 04, 2011

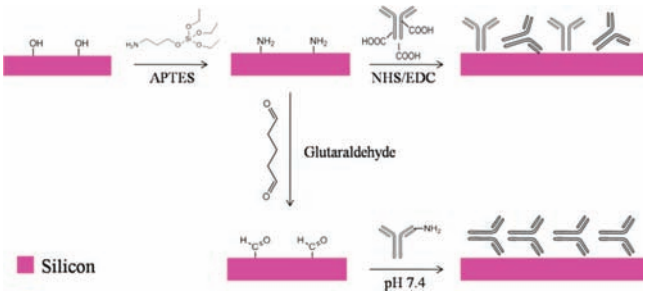


**Figure 1.** Antibody Immobilization. Schemes of antibody immobilization on the sensor surface resulting in different antibody arrangement. Antibodies are immobilized either by the C-terminus or carboxylate containing side chains using NHS/EDC chemistry, or the N-terminus using glutaraldehyde.

screened by measuring both dry and wet current−voltage ($I-V$) characteristics using a custom-made multiplexing system with a National Instruments Data Acquisition (DAQ) Card, NI PCI-6251, and an Agilent 4156 Semiconductor Parameter Analyzer. Typical leakage currents measured are on the order of 100 fA.

Anti-CA15.3 (Alpha Diagnostics) was immobilized on the nanoribbon surface by coupling to either the C- or N- terminus, Figure 1.[17−19] Coupling to APTES-functionalized devices via the C-terminus was achieved using *N*-hydroxysulfosuccinimide and 1-ethyl-3-(3-dimethylaminopropyl) carbodiimide hydrochloride (NHS/EDC) chemistry in 1× phosphate buffered saline (PBS; Sigma) at pH 7.4. Samples were then washed with 1× PBS and blocked with 10% fetal bovine serum (FBS) for 30 min, followed by washing with sensing buffer (1 mM bicarbonate buffer at pH 9). Because of nonselectivity of the NHS/EDC chemistry, the surface configuration of the antibodies results in an ensemble of different orientations due to the coupling of the C-terminus and side chain carboxylic groups with the sensor surface. To couple the antibody via N-terminus, APTES-functionalized devices were immersed in a 5% glutaraldehyde solution in deionized (DI) water for 2 h at room temperature, Figure 1. After washing with 1× PBS, the device surface was reacted with anti-CA15.3 in 1× PBS at pH 7.4 for 2 h, to yield a different antibody arrangement on the surface.[19] A pH of 7.4 ensures that the N-terminus is deprotonated (available for reaction) and the side chain amines are protonated (unavailable for reaction), whereas higher pH (i.e., pH 9.0) would allow all amines (N-terminus and lysine side chains) to be deprotonated (thus an ensemble of configurations). Thus, this allows the bound antigen to be in closer proximity to the sensor surface and be less affected by Debye screening. Unreacted glutaraldehyde was quenched with ethanolamine and the surface was subsequently washed with PBS. The sample was then blocked with 10% FBS for 30 min, followed by washing with 1 mM bicarbonate sensing buffer. Following washing of all samples, 10 $\mu$L of sensing buffer was left in the mixing chamber. Sensing measurements were performed using the DAQ system with $V_{ds}$ = 0.2 V, $V_{backgate,s}$ = −3 V, $V_{solutiongate,s}$ = 0 V, and a sampling rate of 0.5 s. A total of 10 $\mu$L of an antigen solution was injected after establishing a stable baseline current.

The response of an anti-CA15.3-functionalized sensor to the addition of 10 $\mu$L of 50 U/mL CA15.3 in 1 mM bicarbonate buffer at pH 9 ($\lambda_D$ = 9.7 nm) is given in Figure 2, top panel. The binding of the negatively charged antigen—the

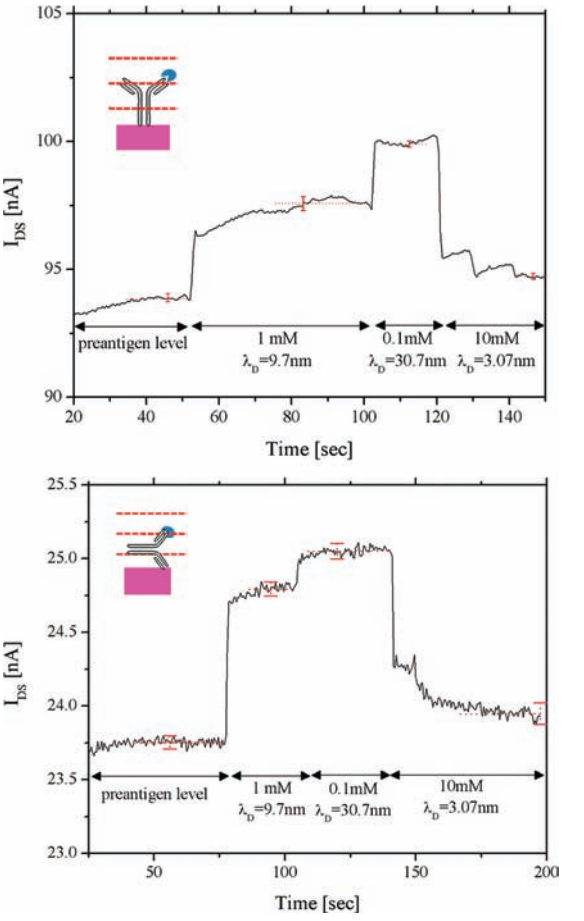


**Figure 2.** Debye length modulation. Time domain device response after antigen injection in 1 mM sensing buffer, followed by a buffer exchange to 0.1 and 10 mM for devices functionalized with anti-CA15.3 via their (top) C-terminus or (bottom) N-terminus. The dotted red line depicts average current value; the vertical line represents variance of device current. Insets show nonlinear fit of device signal change versus the Debye length according to eq 3.

isoelectric point, p*I*, of CA15.3 is <5 [20]—causes an increase in the current of the p-type device. After the device current stabilizes, the 1 mM buffer was exchanged with a 0.1 mM bicarbonate buffer with the same pH, thereby increasing the Debye length to 30.7 nm. This exposes more of the antigen's charge to the sensor, further increasing device current, Figure 2, top panel. The buffer was then replaced with a 1 mM bicarbonate buffer with 10 mM NaCl at pH 9 ($\lambda_D$ = 3 nm). The resulting increase in ionic screening causes a steep decline in current since the Debye length for this ionic strength is shorter than the typical antibody size. Furthermore, since Debye screening exhibits an exponential behavior, the current does not fully drop to the preantigen binding level. The same buffer exchanges were performed on sensors in which the anti-CA15.3 was bound through its N-teminus, Figure 2, bottom panel.

It is important to notice that the buffer exchange will not affect the amount of bound charge as long as the dissociation time of the antigen is much longer than the typical time scale for these experiments (see Supporting Information).

A previous theoretical study[16,21] showed that the nanowire sensitivity factor, the percentage of induced change, to Debye

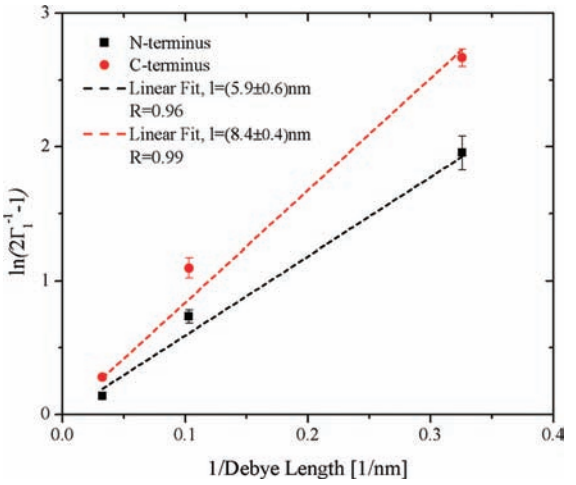


**Figure 3.** Linearized dependence of the sensitivity factor $\Gamma_l$ (eq 3) as a function of Debye length of the sensing buffer for different schemes of functionalization compared to theory.

screening is

$$\Gamma_l \approx 2\frac{R}{R+l}\left[1+\sqrt{\frac{R}{R+l}}\exp\left(\frac{l}{\lambda_D}\right)\right]^{-1} \quad (2)$$

where $R$ is the nanowire diameter, $l$ is the distance from nanowire surface to the surface charge density ($\sigma$, assumed to be homogenously distributed), and $\lambda_D$ is the solution Debye length. To transition to a planar nanoribbon sensor, we let $R \rightarrow \infty$ in eq 2 which yields:

$$\Gamma_l \approx 2\left[1+\exp\left(\frac{l}{\lambda_D}\right)\right]^{-1} \quad (3)$$

Since the nanoribbon current is proportional to $\Gamma_l$ (see Supporting Information), one can determine $l$ from the experimental data of Figure 2 by:

$$\frac{\Delta I}{\Delta I_{max}} = \frac{I(\lambda_D)-I_0}{\Delta I_{max}} = \Gamma_l = 2\left[1+\exp\left(\frac{l}{\lambda_D}\right)\right]^{-1} \quad (4)$$

where $I_0$ is device baseline current prior to antibody binding, $I(\lambda_D)$ is the device current at a specific Debye screening length $\lambda_D$, and $\Delta I_{max}$ is the maximum current change valid for $\lambda_D \rightarrow \infty$. With the use of the proposed theory and a nonlinear least-squares method, we estimate that $\Delta I_{max}$ = 7.3 nA, Figure S2a in Supporting Information. Similarly, using the data in Figure S2b, we estimate that $\Delta I_{max}$ = 1.52 nA for N-terminal antibody functionalization.

Ideally when the surface charge density is located at the nanosensor surface, one can estimate the upper boundary for $\Delta I_{max}$ for a specific device. We use the approximation that $\Delta I_{max} = (\partial I/\partial\psi_0)\Delta\psi_0$ (see Supporting Information), where $\psi_0$ is sensor/solution interface potential and the derivative represents the solution-gate transconductance of the device. The relationship between the surface charge density, $\sigma_0$, of the bound molecules on the sensor surface and the potential at the sensor/solution interface, $\psi_0$,[7] with respect to the reference electrode is

$$\sigma_0 = \sqrt{8\varepsilon_0\varepsilon_W k_B T c_0}\sinh\left(\frac{e\psi_0}{2k_B T}\right) \quad (5)$$

where $\varepsilon_0$ is the vacuum permittivity, $\varepsilon_W$ is the relative permittivity, $k_B$ is the Boltzmann constant, $T$ is the temperature, and $c_0$ is the density of ionic species in the solution. The change in the nanosensor's surface potential, $\Delta\psi_0$, is caused by antigen binding and change of surface charge density. The change of surface charge density is equal to the charge of bound antigens per surface area. This value is estimated to be approximately −10e using the Scripps Institute Protein Calculator v3.3 at pH 9 and the UniProt peptide sequence library. This can be approximated by $\Delta\sigma_0 \sim -2e/nm^2$, where $e$ is the unit charge. Using $\varepsilon_W = 80$, $c_0 = 6 \times 10^{23}$ m$^{-3}$, and $k_BT/e = 26$ mV, we estimate $\Delta\psi_0 = 30$ mV. The solution gate transconductance of the device shown in Figure 2 (bottom panel) is approximately 80 nA/V, Figure S1 in Supporting Information. This yields $\Delta I_{max} \sim 2.4$ nA and is in good agreement with the value obtained from experimental data $\Delta I_{max}$ = 1.52 nA.

With the data from multiple devices and the linearized eq 3, we obtained values for the bound charge average distance from the nanosensor surface, $l$ = (8.4 ± 0.4) nm and $l$ = (5.9 ± 0.6) nm for the C- and N-termini-bound antibodies, respectively. These results are summarized in Figure 3. $\Gamma_l$ is calculated using the eq 4 as $\Delta I/\Delta I_{max}$. The result obtained for C-terminus functionalized devices are in agreement with the value obtained using atomic force microscopy.[22] The error bars are calculated in terms of the standard error of the mean. The estimated lengths are in excellent agreement with typical antibody−antigen complex dimensions, specifically their height and diameter, respectively. Therefore, this approach enables a measurement of the average distance (with respect to the sensor surface) of charged species in receptor−ligand complexes.

By definition $\Gamma_l$ describes the percentage of the surface charge seen by the device in the presence of Debye screening; therefore ,it describes the percentage of the unscreened signal at given Debye length, $\Delta I/\Delta I_{max}$. We estimate that ∼50 ± 3% (5 total devices) of antigen charge is exposed to the sensor (i.e., unscreened) when using 1 mM bicarbonate sensing buffer for C-termini-functionalized antibodies. The shown error is calculated in terms of the standard error of the mean (SEM). Through using N-terminal functionalization, the percentage of exposed charge increased to ∼65 ± 2% (5 total devices). This demonstrates the influence of binding site distance from the sensor surface on signal detection, resulting from differences in antibody configuration.

## CONCLUSION

In this work, we demonstrate that Debye screening manipulation can be employed for quantitative spatial analysis of induced charge on a nanosensor surface. The model system used in this manuscript was a functionalized receptor (antibody)−target ligand (antigen), but the approach detailed here holds for any bound charged moiety. Specifically, we show that different configurations of receptors can be distinguished by the Debye screening manipulation method. In addition to the enhanced quantitative understanding of analyte−receptor spatial configuration, this approach also opens new directions for FET based nanosensor applications, such as observing dynamic conformational changes in biomolecules. Our results further demonstrate the critical dependence of sensitivity on receptor orientation, highlighting the importance of functionalization chemistries.

## ■ ASSOCIATED CONTENT

**Supporting Information.** Device $I_d - V_{sg}$ (current-solution gate) characteristics and solution transconductance; analysis of time-domain sensograms. Derivation and analysis of eqs 2−4; surface plasmon resonance sensograms and analysis of antigen dissociation kinetics; derivation of the relation between the current change ($\Delta I_{max}$), solution transconductance ($g_m$), and sensor surface potential variation ($\Delta\psi_0$). This material is available free of charge via the Internet at http://pubs.acs.org.

## ■ AUTHOR INFORMATION

**Corresponding Author**
aleksandar.vacic@yale.edu; mark.reed@yale.edu

## ■ ACKNOWLEDGMENT

We thank Weihua Guan and Yeonwoong (Eric) Jung for helpful discussion, Mike Power of the Yale SEAS Cleanroom and Dr. Rob Ilic of Cornell Nanofabrication Facility for device processing assistance and discussion. We thank Dr. Ewa Folta-Stogniew and the Biophysics Resource of the W.M. Keck Biotechnology Laboratory at Yale School of Medicine which is supported by the NIH Award Number RR026992. This work was partially supported by the National Institutes of Health (NIH R01EB008260), DTRA (HDTRA1-10-1-0037), ARO (W911NF-08-1-0365), the Canadian Institute for Advanced Research (CIfAR).

## ■ REFERENCES

(1) Moss, S. D.; Curtis, J. J.; Johnson, C. *Anal. Chem.* **1975**, *47*, 2238–2242.
(2) Patolsky, F.; Lieber, C. M. *Mater. Today* **2005**, *8*, 20–28.
(3) Stern, E.; Klemic, J. F.; Routenberg, D. A.; Wyrembak, P. N.; Turner-Evans, D. B.; Hamilton, A. D.; LaVan, D. A.; Fahmy, T. M.; Reed, M. A. *Nature* **2007**, 519–522.
(4) Bunimovitch, Y. L.; Shin, Y. S.; Yeo, W.-S.; Amori, M.; Kwong, G.; Heath, J. R. *J. Am. Chem. Soc.* **2006**, 16323–16331.
(5) Stern, E.; Steenblock, E. R.; Reed, M. A.; Fahmy, T. M. *Nano Lett.* **2008**, *8*, 3310–3314.
(6) Patolsky, F.; Lieber, G. Z. C. M. *Anal. Chem.* **2006**, *78*, 4260–4269.
(7) Israelachvili, J. *Intermolecular & Surface Forces*; Academic Press: London, 1991.
(8) Li, Z.; Chen, Y.; Li, X.; Kamins, T. I.; Nauka, K.; Williams, R. S. *Nano Lett.* **2004**, *4*, 245–247.
(9) Zhang, G.-J.; Zhang, G.; Chua, J. H.; Chee, R.-E.; Wong, E. H.; Agarwal, A.; Buddharaju, K. D.; Singh, N.; Gao, Z.; Balasubramanian, N. *Nano Lett.* **2008**, *8*, 1066–1070.
(10) Lud, S. Q.; Nikolaides, M. G.; Haase, I.; Fischer, M.; Bausch, A. R. *ChemPhysChem* **2006**, 379–384.
(11) Nair, P. R.; Alam, M. A. *IEEE Trans. Electron Devices* **2007**, *54*, 3400–3408.
(12) Stern, E.; Wagner, R.; Sigwort, F. J.; Breaker, R.; Fahmy, T. M.; Reed, M. A. *Nano Lett.* **2007**, *7*, 3405–3409.
(13) Elfstrom, N.; Karlstrom, A. E.; Linnros, J. *Nano Lett.* **2008**, *8*, 945–949.
(14) Stern, E.; Vacic, A.; Rajan, N. K.; Criscione, J. M.; Park, J.; Ilic, B. R.; Mooney, D. J.; Reed, M. A.; Fahmy, T. M. *Nature Nanotechnol.* **2010**, 138–142.
(15) Vacic, A.; Criscione, J. M.; Rajan, N. K.; Fahmy, T. M.; Reed, M. A. In *APS March Meeting*, Dallas, TX, 2011.
(16) Sorensen, M. H.; Mortensen, N. A.; Brandbyge, M. *Appl. Phys. Lett.* **2007**, *91*, 102105.
(17) Nagare, G. D.; Mukherji, S. *Appl. Surf. Sci.* **2009**, 3696–3700.
(18) Weiping, Q.; Bin, X.; Lei, W.; Chunxiao, W.; Zengdong, S.; Danfeng, Y.; Zuhong, L.; Yu, W. *J. Inclusion Phenom. Macrocyclic Chem.* **1999**, 419–429.
(19) Selo, I.; Negroni, L.; Creminon, C.; Wal, J. M. *J. Immunol, Methods* **1996**, *199*, 127–138.
(20) Wu, J.; Yan, Y.; Yan, F.; Ju, H. *Anal. Chem.* **2008**, 6072–6077.
(21) De Vico, L.; Sorensen, M. H.; Iversen, L.; Rogers, D. M.; Sorensen, B. S.; Brandbyge, M.; Nygard, J.; Martinez, K. L.; Jensen, J. H. *Nanoscale* **2011**, *3*, 706–717.
(22) Park, C. W.; Ah, C. S.; Ahn, C.-G.; Yang, J.-H.; Kim, A.; Kim, T.; Sung, G. Y. In *Proceedings of the Eurosensors XXIII conference, Procedia Chemistry*; Elsevier: 2009; Vol. 1, pp 674−677.